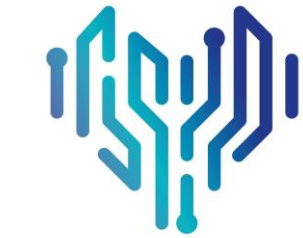

SIMCor

In-Silico testing and validation of Cardiovascular IMplantable devices

Call: H2020-SC1-DTH-2018-2020 (*Digital transformation in Health and Care*)

Topic: SC1-DTH-06-2020 (*Accelerating the uptake of computer simulations for testing medicines and medical devices*)

Grant agreement No: 101017578

Deliverable 6.3

Uncertainty quantification for input data

Due date of delivery: 30 September 2022

Actual submission date: 22 September 2022

Start of the project: 1 January 2021
End date: 31 December 2023

This project has received funding from the European Union's Horizon 2020 research and innovation programmeunder grant agreement N° 101017578

Reference

Name	SIMCor_D6.3_Uncertainty quantification for input data_CHA_22-09-2022
Lead beneficiary	Charité – Universitätsmedizin Berlin (CHA)
Author(s)	Leonid Goubergrits (CHA), Nina Krüger (CHA), Jan Brüning (CHA)
Dissemination level	Public
Type	Report
Official delivery date	30 September 2022
Date of validation by the WP Leader	22 September 2022
Date of validation by the Coordinator	22 September 2022
Signature of the Coordinator	Jan Bruening Digital unterschrieben von Jan Bruening Datum: 2022.09.22 00:22:54 +02'00'

Version log

Issue date	Version	Involved	Comments
17/08/2022	1.0	Leonid Goubergrits (CHA), Nina Krüger (CHA),	First draft by CHA
16/09/2022	2.0	Wouter Huberts (TUE)	Internal review by TUE
20/09/2022	3.0	Jan Brüning (CHA), Leonid Goubergrits (CHA), Nina Krüger (CHA),	Implementation of changes and suggestions done by the internal review
21/09/2022	4.0	Anna Rizzo (LYN)	Project Manager's review
22/09/2022	Final	Jan Brüning (CHA)	Submission by PC

Executive summary

This document describes the uncertainty analysis of geometrical and functional model input data obtained by processing of either *computed tomography* (CT) or *magnetic resonance imaging* (MRI) data as well as sensor data. Uncertainties introduced during this image or sensor data processing phase might propagate to uncertainties in calculated parameters and boundary conditions, either modelled or directly measured, for simulations. In addition, possible uncertainties in geometry-derived morphometric or hemodynamic parameters are assessed. Uncertainty quantification of input data used to set boundary conditions in simulations is an essential part validating the proposed simulation methods within SIMCor as part of *WP6 - Data processing for anatomy and function*.

Table of contents

INTRODUCTION **6**

DEFINITION OF SUB-COHORTS FOR UNCERTAINTY QUANTIFICATION **8**

SUB-COHORT OF PATIENTS USED FOR UNCERTAINTY QUANTIFICATION OF THE PA 8
SUB-COHORT OF PATIENTS USED FOR UNCERTAINTY QUANTIFICATION OF THE AV 8
VALIDITY OF THE SUB-COHORTS 8

EXTRACTION OF ANATOMICAL INPUT DATA FROM IMAGE DATA **9**

PA SEGMENTATION USING MANUAL APPROACH 9
PA SEGMENTATION USING MACHINE LEARNING 11
EXTRACTION OF THE PA GEOMETRIC PARAMETERS 12
SEGMENTATION OF THE AV USING PARAMETRIC HEART MODEL 14
QUANTIFICATION OF AV CALCIFICATION 15

EXTRACTION OF HEMODYNAMIC BLOOD FLOW INFORMATION **16**

CATHETER-BASED PRESSURE MEASUREMENTS **17**

UNCERTAINTY QUANTIFICATION OF SEGMENTATIONS **18**

UNCERTAINTY QUANTIFICATION OF MANUALLY SEGMENTED PA SURFACES 18
UNCERTAINTY QUANTIFICATION OF GEOMETRIC PARAMETERS: MANUAL PA RECONSTRUCTION 18
UNCERTAINTY QUANTIFICATION OF PA SURFACES: MANUAL VS. AUTOMATIC RECONSTRUCTION 20
UNCERTAINTY QUANTIFICATION OF PA GEOMETRIC PARAMETERS: MANUAL VS. U-NET SEGMENTATIONS 20
UNCERTAINTY QUANTIFICATION OF THE AV AREA 21
UNCERTAINTY QUANTIFICATION OF THE AV CALCIFICATION VOLUME 21

UNCERTAINTY QUANTIFICATION OF PA FLOW RATES **22**

UNCERTAINTY ANALYSIS OF CATHETER-MEASURED PRESSURE CURVES **23**

CONCLUSIONS **24**

APPENDIX **25**

LIST OF TOOLS USED FOR UNCERTAINTY QUANTIFICATION 25
LIST OF PARAMETERS USED FOR UNCERTAINTY QUANTIFICATION 25

List of figures

FIGURE 1: GEOMETRY RECONSTRUCTION WORKFLOW: (A) ONE ORTHOGONAL SLICE OF THE CT IMAGING DATA OF A SHEEP; (B) BLUE COLOUR MARKS AUTOMATIC SELECTION OF ALL VOXELS IN THE SLICE WITH HU ABOVE 175; (C) RED-SHARPENED AREA MARKS PA LUMEN IN THE SLICE AFTER THE MANUAL INTERACTION SELECTION; (D) LABEL VOXEL FIELD OF THE PA WITH A VOXEL SIZE OF 0.75MM X 0.75MM X 0.75MM; (E) ROUGH TRIANGULATED SURFACE RECONSTRUCTION WITH STEP ARTEFACTS; (F) FINAL VOLUME PRESERVED SMOOTHED SURFACE OF THE PA. 9
FIGURE 2: FOUR PA SURFACE GEOMETRIES RECONSTRUCTED BY 2 INDEPENDENT OPERATORS: OPERATOR 1 - UPPER ROW, OPERATOR 2 - LOWER ROW. 10
FIGURE 3: EXEMPLARY VOXEL MASK USED FOR TRAINING OF THE NNU-NET. 11
FIGURE 4: FOUR PA SURFACE GEOMETRIES MANUALLY RECONSTRUCTED BY ONE OPERATOR (UPPER ROW) AND AN AUTOMATED APPROACH USING A NEURAL NETWORK (LOWER ROW). 11
FIGURE 5: LEFT: EXAMPLE OF 2 SUPERIMPOSED SURFACE GEOMETRIES OF THE PA RECONSTRUCTED BY TWO INDEPENDENT OPERATORS (RED SURFACE - OPERATOR 1; PURPLE SURFACE - OPERATOR 2). RED AND PURPLE BOUNDING BOXES SHOW MINOR DIFFERENCES IN RECONSTRUCTED DOMAINS, WHICH RESULTS, HOWEVER, IN A LARGE HAUSDORFF DISTANCE OF 13 MM, WHILE THE MEAN AND STANDARD DEVIATION OF THE SURFACE DISTANCE WAS 0.27 MM AND 1.08 MM, RESPECTIVELY. THE BLACK FRAME IN THE LEFT PANEL SHOWS THE REGION OF INTEREST (ROI) USED FOR THE SURFACE DISTANCE ANALYSIS RESULTING IN A HAUSDORFF DISTANCE OF 1.34 MM AND MEAN AND STANDARD DEVIATION OF THE SURFACE DISTANCE OF 0.23 MM AND 0.25 MM RESPECTIVELY, WHICH IS SMALLER THAN THE AVERAGE VOXEL SIZES 12

FIGURE 6: MEASUREMENTS FROM CENTRELINE-BASED ANALYSIS: THE CENTRELINE (RED) IS SUBDIVIDED INTO SEVERAL EDGES, CONNECTED BY NODES (BLUE), WHICH MARK A BIFURCATION. DIAMETERS FOR EACH EDGE ARE OBTAINED AT THE MIDPOINT (BLUE STAR) BETWEEN START AND END NODE OF AN EDGE OR AT START NODE + 0.8 * (END NODE - START NODE) FOR BRANCHES (BLUE TRIANGLE). THE BIFURCATION ANGLE BETWEEN LPA AND RPA IS THE ANGLE BETWEEN THE VECTORS CONNECTING THE ENDPOINT OF THE MPA TO THE ENDPOINT OF THE FIRST EDGE OF LPA AND RPA, RESPECTIVELY. 13
FIGURE 7: ASSESSMENT OF AV CALCIFICATION: (A) - CT IMAGE DEPICTING THE AV AND A BLACK ARROW HIGHLIGHTING CALCIFICATIONS WITH HIGH HOUNSFIELD UNIT VALUES. (B) - VISUALISATION OF THE AV AS AN ISOSURFACE WITH A CONSTANT HU OF 400 AND BLACK WIREFRAME DEFINING THE ROI USED FOR THE CALCIFICATION VOLUME MEASUREMENT. (C) AND (D) - FRONTAL AND BACK SURFACES OF THE AV (RED) AS WELL AS CALCIFICATIONS (BLUE). 15
FIGURE 8: EXEMPLARY 4D VELOCITY ENCODED MRI VELOCITY VECTOR FIELD IN THE PA WITH A MEASUREMENT PLANE PERPENDICULAR TO MPA. 16
FIGURE 9: EXEMPLARY CATHETER-MEASURED PRESSURE CURVES IN THE LEFT VENTRICLE (LEFT) AND THE ASCENDING AORTA (RIGHT). RED DOTS MARK PEAK SYSTOLIC VALUES. 17
FIGURE 10: SCATTER PLOTS AND LINEAR REGRESSION ANALYSIS FOR FOUR EXEMPLARY GEOMETRIC PARAMETERS DESCRIBING THE PA ANATOMY. OPERATOR 1 - O1. OPERATOR 2 - O2. CURVATURE INDEX - CI. 19
FIGURE 11: LEFT: THE FIRST PLANE FOR FLOW RATE MEASUREMENT IN THE MPA TOGETHER WITH THE MEASURED FLOW RATE CURVE. RIGHT: THE LAST PLANE FOR THE MPA FLOW RATE MEASUREMENTS WITH THE RESPECTIVE CURVE. 22

List of tables

TABLE 1: COMPARISON OF SELECTED PARAMETERS BETWEEN THE WHOLE COHORT OF SEGMENTED HUMAN PA AGAINST THE SUB-COHORT OF 10 PATIENTS USED FOR THE UNCERTAINTY ANALYSIS. 8
TABLE 2: COMPARISON OF SELECTED PARAMETERS BETWEEN THE WHOLE COHORT OF RECONSTRUCTED HUMAN AV WITH THE SUB-COHORT USED FOR UNCERTAINTY ANALYSIS (TPGCATH: CATHETER-MEASURED TRANSVALVULAR MAXIMAL PRESSURE GRADIENT; AVA: AV AREA). 8
TABLE 3: ANALYSIS OF THE SURFACE DISTANCES BETWEEN MANUAL PA RECONSTRUCTIONS OF 10 HUMAN CASES BY 2 INDEPENDENT OPERATORS IN A LIMITED REGION OF INTEREST WHICH REPRESENTS ONLY THE MOST RELEVANT ANATOMICAL REGION INCLUDING MAIN, LEFT, AND RIGHT PA BUT NOT ALL BRANCHING VESSELS. 18
TABLE 4: RELATIVE UNCERTAINTIES DUE TO MANUAL SEGMENTATIONS PERFORMED BY TWO OPERATORS OF THE FOUR EXEMPLARY GEOMETRIC PARAMETERS: MPA LENGTH (L), BIFURCATION ANGLE (α) BETWEEN LEFT AND RIGHT PA, LPA DIAMETER (D), AND RPA CURVATURE INDEX (CI). 19
TABLE 5: ANALYSIS OF THE SURFACE DISTANCES BETWEEN MANUAL AND AUTOMATIC PA RECONSTRUCTIONS OF ALL 10 HUMAN CASES IN A LIMITED REGION OF INTEREST WHICH REPRESENTS ONLY THE MOST RELEVANT ANATOMICAL REGION INCLUDING MAIN, LEFT, AND RIGHT PA BUT NOT ALL BRANCHING VESSELS. 20
TABLE 6: RELATIVE UNCERTAINTIES DUE TO MANUAL RECONSTRUCTION PERFORMED BY OPERATOR 1 AND AUTOMATIC RECONSTRUCTIONS, CALCULATED FOR FOUR EXEMPLARY GEOMETRIC PARAMETERS: MAIN PA (MPA) LENGTH (L), BIFURCATION ANGLE (α) BETWEEN LEFT AND RIGHT PA (RPA), LPA DIAMETER (D), AND RPA CURVATURE INDEX (CI)..... 20
TABLE 7: RESULTS OF THE CALCIFICATION VOLUME QUANTIFICATION AND RESULTING RU EXEMPLARY FOR 3 TAVI PATIENTS. 21
TABLE 8: EXEMPLARY PA FLOW RATES MEASURED FOR THREE SUBJECTS. MEAN AND PEAK-SYSTOLIC FLOW RATES AVERAGED OVER MEASUREMENTS IN 10 DIFFERENT PLANES ALONG THE MPA, AS WELL AS THE RELATIVE UNCERTAINTIES CALCULATED FOR BOTH PARAMETERS..... 22
TABLE 9: PEAK SYSTOLIC PRESSURES AND SYSTOLIC TIMES AVERAGED OVER CATHETER-BASED PRESSURE MEASUREMENTS OF FIVE CONSECUTIVE HEART CYCLES IN 5 TAVI PATIENTS WITH RESULTING RU FOR PRESSURE AND TIME..... 23
TABLE 10: LIST OF USED TOOLS. 25
TABLE 11: LIST OF INVESTIGATED PARAMETERS. 25

Acronyms

Acronym	Full name
AV	Aortic valve
CHA	Charité - Universitätsmedizin Berlin
CT	Computed tomography
HU	Hounsfield unit
ICC	Intraclass correlation coefficient
LV	Left ventricle
LPA	Left pulmonary artery
MPA	main pulmonary artery
MRI	Magnetic resonance imaging
PA	Pulmonary artery
PAPS	Pulmonary artery pressure sensor
RPA	Right pulmonary artery
ROI	Region of interest
RU	Relative uncertainty
s.d.	Standard deviation
TAVI	Transcatheter aortic valve implantation
TUE	Technische Universität Eindhoven
UA	Uncertainty analysis
VEC	Velocity encoding

Introduction

One major aim of SIMCor is to investigate to what extent numerical simulations can support and enhance development and certification of implantable cardiovascular devices. Here, two use cases were defined. The first use case focuses on the evaluation of heart valve prostheses that can be implanted in a minimally invasive way via cardiac catheterization (i.e., *transcatheter aortic valve implantation*, TAVI). These prostheses are used to replace the native *aortic valve* (AV) in case it is diseased. The second use case deals with *pulmonary artery pressure sensors* (PAPS) that can be implanted into the *pulmonary artery* (PA), again using catheterization, to monitor PA pressure, which is a relevant diagnostic parameter in patients with heart failure.

While TAVI is a relatively young technique, it had a disruptive effect on treatment of AV disease and is already performed more frequently than surgical implantation of AV prostheses[1]. The already large number of devices is steadily increasing. In contrast, the first and only PAPS device to date received premarket approval by the US American Food and Drug Administration in 2011[2]. As both devices are implanted into the cardiovascular system, their requirements regarding safety and efficacy due to interaction with flowing blood are high. This is associated with large efforts and high costs in development, testing and certification.
Numerical methods for simulation of mechanical or hemodynamical properties of the cardiovascular system with or without artificial organs or medical devices became increasingly important for academic as well as industrial research. Also, first numerical models used for diagnosis of cardiovascular diseases successfully reached the market and received clearance by regulatory bodies of almost all industrialised nations[3]. These methods hold the potential to also simulate the interaction between medical devices and the patient-specific cardiovascular system and thus predict the post-treatment outcome.

To investigate these interactions between device, tissue and blood using in-silico modelling, the relevant region of interest of the patient-specific cardiovascular system must be described as detailed as possible. Here, the most relevant information includes patient-specific anatomy of the aorta, the left ventricular outflow tract, and the AV for modelling of TAVI implantation and efficacy, and of the PA for modelling of PAPS implantation and efficacy. This information is usually acquired from various imaging modalities such as CT, MRI, or echocardiography. Additionally, medical image technologies also allow, at least to a given extent, to assess patient-specific functional information on blood flow, such as velocity profiles, flow rates, flow rate divisions and the stroke volumes of the left and right ventricle. The latter type of information is necessary for providing accurate boundary conditions to the numerical simulations.

All steps of the modelling pipeline, starting from medical image data acquisition, can affect simulation results. However, medical image acquisition is usually a well-established routine procedure, following acquisition protocols defining requirements for image data quality as well as for spatiotemporal resolution. In the frames of *D6.1 - Specification of data-processing requirements (CHA, M4)*, requirements for medical image data to be processed within SIMCor were described.
In the following section, the key procedure - the extraction of the anatomical or hemodynamic information from image data - and their uncertainties, which are mostly associated with operator biases, are investigated in the human sub-cohorts. In the project, different processing procedures

[1] https://www.herzstiftung.de/e-paper/#0; page 83.

[2] Ayyadurai P, Alkhawam H, Saad M, Al-Sadawi MA, Shah NN, Kosmas CE, Vittorio TJ. An update on the CardioMEMS pulmonary artery pressure sensor. Ther Adv Cardiovasc Dis. 2019 Jan-Dec;13:1753944719826826. doi: 10.1177/1753944719826826. PMID: 30803405; PMCID: PMC6376505.

[3] https://www.heartflow.com/.

were used, including manual and fully automated segmentation of *pulmonary arteries* (PA), automatic segmentation of the *left ventricle* (LV), the AV and the aorta by using a parametric model, as well as a manual correction of the AV leaflets.

Definition of sub-cohorts for uncertainty quantification

Sub-cohort of patients used for uncertainty quantification of the PA

In SIMCor PA of 50 patients were segmented manually from CT data for subsequent use in WP8 and WP9, focussing on numerical modelling of the PAPS device implantation, device effect and efficacy. For this, the interaction between the device and the tissue of the PA but also between the device and the bloodstream must be modelled. To quantify the uncertainty of the segmentation procedure and the impact of this uncertainty on the assessment of morphometric and hemodynamic parameters of interest, 10 cases were selected randomly and segmented again by a second operator (inter-operator bias). There were no relevant differences between the demographic and anatomical parameters of the sub-cohort and the entire cohort (Student's t-test, $p > 0.05$; see *Table 1*). Both operators performing the manual reconstruction for assessing the operator bias had long-standing experience in image-based processing of different anatomical structures of the cardiovascular system of more than 10 years. In addition to the manual reconstruction, a machine learning-based approach using a standard 'U-net' architecture was evaluated for reconstruction of the patient-specific PA anatomy.

	N of cases	Sex (% male)	Age (years)	Weight (kg)	BSA (m^2)	BMI (kg/m^2)	MPA length (mm)	MPA diameter (mm)
Sub-cohort	10	70%	81±4.8	83±21.1	1.95±0.23	28.7±7.0	41.6±7.4	31.3±4.2
Cohort	48	60%	81±7.7	77±18.4	1.87±0.24	26.9±5.4	47.1±8.3	31.0±3.8

Table 1: Comparison of selected parameters between the whole cohort of segmented human PA against the sub-cohort of 10 patients used for the uncertainty analysis.

Sub-cohort of patients used for uncertainty quantification of the AV

In SIMCor over 100 individual geometries of patients treated via TAVI were reconstructed from CT data for subsequent use in WP8 and WP9, focussing on numerical modelling of the TAVI device implantation, device effect and efficacy. To quantify segmentation uncertainty, the intra- and inter-operator variability of the reconstruction procedure was quantified in 10 randomly selected cases. No relevant differences between the demographic and anatomical parameters of the sub-cohort and the entire cohort were found (see *Table 2*).

	N of cases	Sex (% male)	Age (years)	Weight (kg)	BSA (m^2)	TPG_{cath} (mmHg)	AVA (cm^2)
Sub-cohort	10	51%	79±7.1	70±16.9	1.79±0.25	43.8±44.1	0.94±0.45
Cohort	101	40%	82±5.5	77±18.6	1.88±0.26	50.5±26.0	0.80±0.25

Table 2: Comparison of selected parameters between the whole cohort of reconstructed human AV with the sub-cohort used for uncertainty analysis (TPGcath: catheter-measured transvalvular maximal pressure gradient; AVA: AV area).

Validity of the sub-cohorts

As in both sub-cohorts no relevant deviations in either relevant anatomical or demographic parameters from the entire cohorts were observed, these cohorts were used for the subsequent uncertainty quantification. As parameter ranges were similar between the entire and the sub-cohorts and the sub-cohorts included ten patients each, findings from these sub-cohorts are generalizable for the entire cohorts.

Extraction of anatomical input data from image data

PA segmentation using manual approach

The end-diastolic 3D geometry of the human PA was segmented and reconstructed from retrospective CT data. CT data sets of the entire heart (*Figure 1*) were acquired from clinical routine, including different clinical indications, as for example TAVI planning.

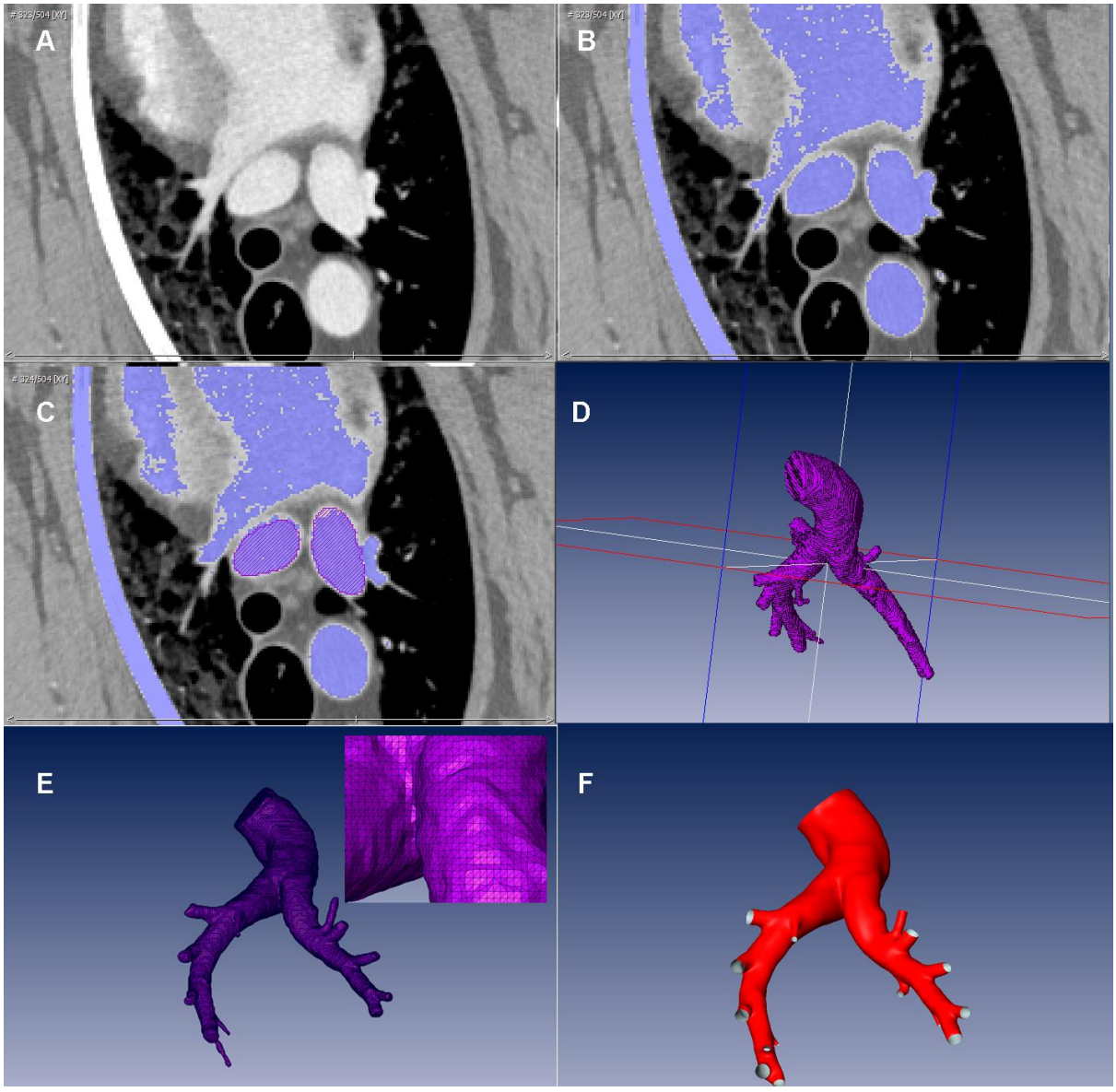

Figure 1: Geometry reconstruction workflow: (A) one orthogonal slice of the CT imaging data of a sheep; (B) regions highlighted in blue are automatically selected voxels in the current slice with an Hounsfield unit value above 175; (C) the two highlighted areas (purple colour, red border) highlight the PA lumen in the current slice; (D) Label voxel field of the PA; (E) rough triangulated surface reconstruction with step artefacts; (F) final volume-preserved smoothed surface of the PA.

Two different wide area-detector volume CT scanners (Aquilion One Vision, Canon Medical Systems; Revolution CT, GE Healthcare, Chicago, IL, USA) with 100kV tube voltage were used for image acquisition. The image resolution varied from (0.390 - 0.648) × (0.390 – 0.648) mm² for the in-plane resolution and between (0.5 - 1.0) mm for the slice thickness.

The manual reconstruction of both operators followed the exact same protocol and was realised using ZIBAmira (v. 2015.28, Zuse Institute Berlin, Germany). To support the manual segmentation, first, all image voxels above a specific Hounsfield Unit (HU) threshold were labelled as candidates for the PA lumen. The threshold definition was patient-specific due to high variability in the contrast agent concentration. The HU threshold varied between 80 and 190. From the remaining image voxels, the PA lumen was reconstructed slice by slice, beginning from RVOT, using the brush as well as the region-growing tools. The segmentation was corrected by slicing through the data stack from top to bottom as well as from left to right and front to back. Multiple iterations were necessary to facilitate the final reconstruction. This approach was necessary, as an automated approach based solely on the HU values would inevitably have resulted in segmentation of the pulmonary veins as well, due to their close proximity to the PA as well as the similar HU values.

The final voxel mask was then used to generate a rough triangulated surface using a Marching Cubes algorithm[4]. Afterward, all geometries were smoothed using a volume-preserving smoothing algorithm[5] implemented in JavaView. Smoothing of the surface geometries was necessary, as the discrete resolution of CT images results in surface mesh geometries with pronounced steps. The volume change between original and smoothed surface geometries was below 0.2%. The average distance between the smoothed and the original surface is below half of the voxel resolution. All geometries were truncated at the *main PA* (MPA) directly after the sinus of the pulmonary trunk, whereas all side branches of the *left PA* (LPA) and *right PA* (RPA) were truncated at the approximately 10 mm length from their origins. The reconstruction workflow is exemplary shown in *Figure 1* for an animal (ovine) data set. Exemplary reconstructions by both operators for four cases of the PA sub-cohort are shown in *Figure 2*.

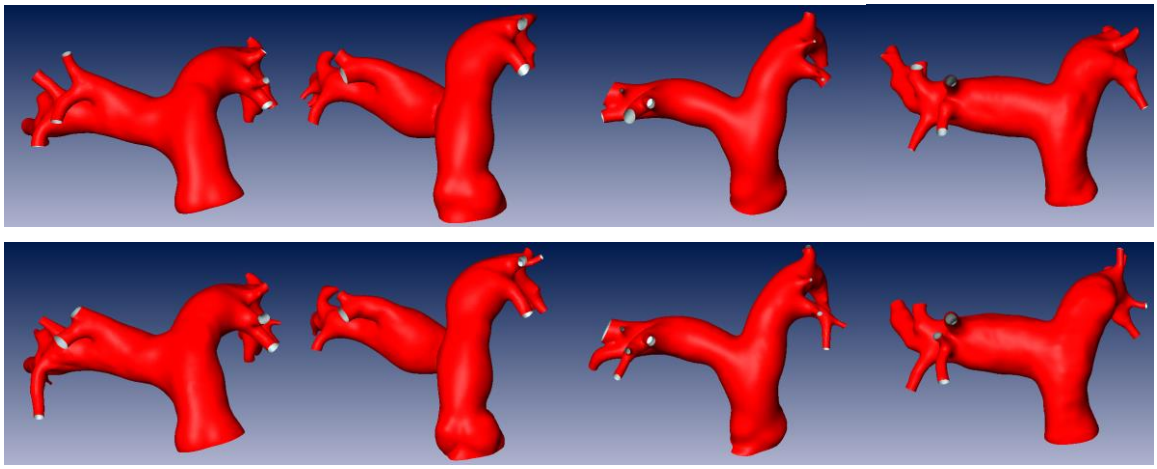

Figure 2: Four PA surface geometries reconstructed by 2 independent operators: Operator 1 - upper row, Operator 2 - lower row.

[4] Lorensen WE, Cline HE. Marching cubes: a high-resolution 3D surface construction algorithm. Proceeding SIGGRAPH '87 Proceedings of the 14th annual conference on Computer graphics and interactive techniques, Pages163–169.

[5] Kuprat, A., Khamayseh, A., George, D. & Larkey, L. Volume conserving smoothing for piecewise linear curves, surfaces, and triple lines. J. Comput. Phys. 172, 99–118. https ://doi.org/10.1006/jcph.2001.6816 (2001).

PA segmentation using machine learning

In addition to the manual segmentation performed by two operators, a machine learning-based method for reconstruction of the PA anatomy was evaluated. Here, a full resolution nnU-Net[6] was trained on PA label masks, available from a previous project. This technique is a self-configuring deep neural network for biomedical image segmentation. Different configurations were tested for pre-processing, network architecture, training and post-processing and the most suitable combination of approaches for the given dataset was selected for inference. The dataset contained 130 CT image data sets. 100 data sets were used for training of the network, while 30 were used for validation. The image resolution, in pixels, were between 512 x 512 x 228 and 512 x 512 x 376, whereas the in-plane voxel resolution was between 0.50 and 0.95 mm, whereas the slice thickness was always 1 mm. *Figure 4* representatively shows PA surfaces of four cases reconstructed by Operator 1 and by the neural network.

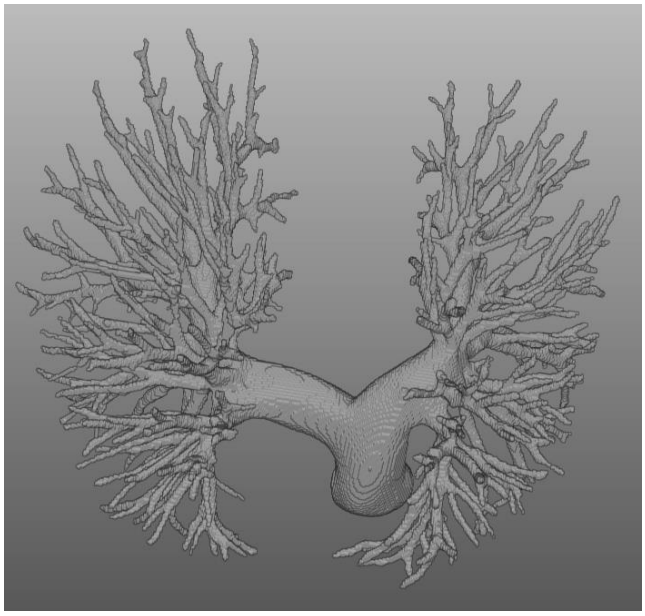

Figure 3: Exemplary voxel mask used for training of the nnU-Net.

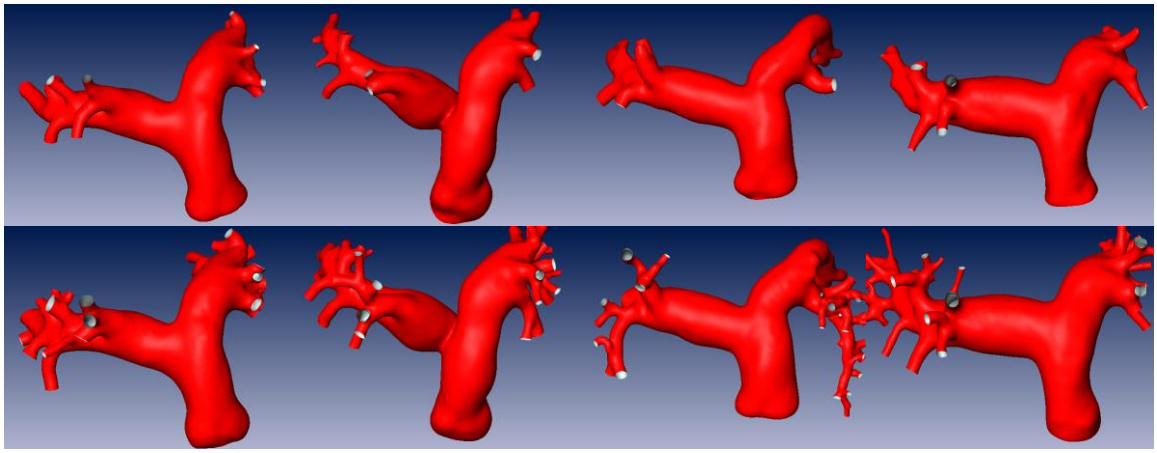

Figure 4: Four PA surface geometries manually reconstructed by one operator (upper row) and an automated approach using a neural network (lower row).

[6] Isensee, F., Jaeger, P. F., Kohl, S. A., Petersen, J., & Maier-Hein, K. H. (2020). nnU-Net: a self-configuring method for deep learning-based biomedical image segmentation. Nature Methods, 1-9.

Extraction of the PA geometric parameters

To quantify differences between different segmentations of the same PA, two approaches were used. First, we performed the assessment of surface differences using -ZIBAmira, a software tool which calculates the mean and standard deviation of the distances between two similar surfaces: an Euclidean surface distance was calculated for each node of the triangulated surface mesh describing the shape of the one of two surfaces, which is defined as the master surface, to the nearest point of the second surface, which is defined as the slave surface (see *Figure 5*). Finally, a Hausdorff distance is calculated. Since manual segmentations often result in different lengths of the segmented outlet branches, in order to avoid the resulting analysis bias we defined a common region of interest for each investigated case.

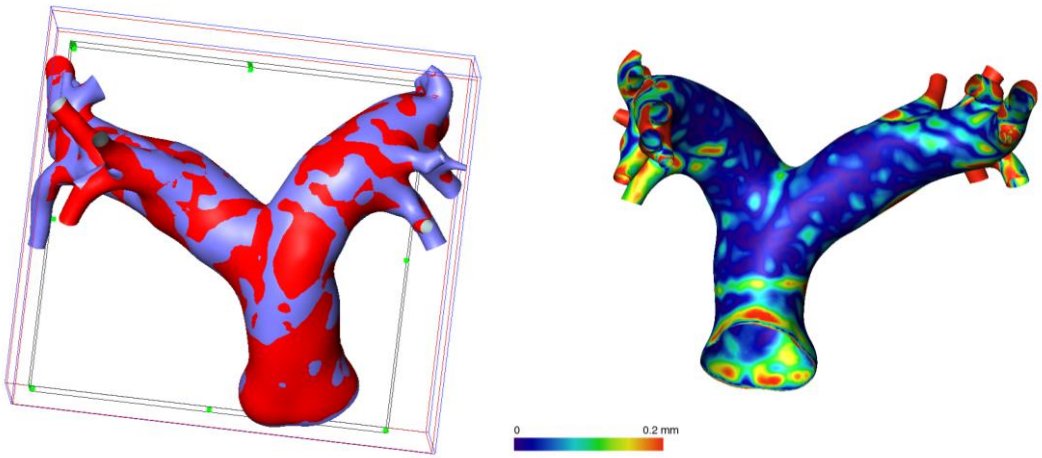

Figure 5: Left: Example of 2 superimposed surface geometries of the PA reconstructed by two independent operators (red surface - Operator 1; purple surface - Operator 2). Red and purple bounding boxes show minor differences in reconstructed domains, which results, however, in a large Hausdorff distance of 13 mm, while the mean and standard deviation of the surface distance was 0.27 mm and 1.08 mm, respectively. The black frame in the left panel shows the region of interest (ROI) used for the surface distance analysis resulting in a Hausdorff distance of 1.34 mm and mean and standard deviation of the surface distance of 0.23 mm and 0.25 mm respectively, which is smaller than the average voxel sizes.

Second, we carried out a paired statistical comparison between geometric parameters, which were selected to describe the PA anatomy. For the analysis, we selected geometric parameters which could potentially affect the safety and function of the implantable PAPS device. There are two major safety and functionality endpoints of interest which affect the selection of the relevant geometric parameters: (1) fixation of the device and (2) thrombosis, which are affected by the complex interaction between the blood flow, the anatomy, and the device.

The stable implantation and fixation of the device is important, as device migration into smaller vessel segments of the PA could result in obstructions of parts of the pulmonary circulation, affecting the lung function, which could be potentially life threatening for patients. From this point of view, diameters of the LPA and RPA, as well as the curvature and ellipticity of these vessel segments are of interest. Furthermore, the implanted device, which is manufactured using non-biological material, is an obstacle for the blood flow in the PA, which results in a disturbed flow with increased turbulence, flow separation and regions of flow recirculation. These disturbed flow features are known to promote thrombus formation, especially in regions with low wall shear stresses. Similarly, geometric parameters, such as the bifurcation angle between LPA and RPA, cross-sectional enlargement from MPA to LPA and RPA, are relevant to device migration. Finally, the lengths of RPA and LPA are of interest for the device implantation procedure.

All measurements were obtained automatically using a centreline-based analysis of reconstructed surface geometries (see *Figure 6*). This analysis was performed using MeVisLab (MeVis Medical Solutions AG, Germany). Centrelines were generated using a shortest path algorithm to connect the midpoint of the opening of the MPA and the midpoints of each branch endpoint. The centrepoints were calculated as the mean of all points on the respective boundary. The shortest paths were accumulated into a single graph, the edges smoothed, unnecessary nodes removed as well as possible cycles reduced to the shortest connection. The root was set to be the midpoint of the MPA and the graph was directed accordingly.

All edges up until the first bifurcation were considered to belong to the MPA. The LPA and RPA were defined depending on the orientation within the scanner. Starting from the first edge of the LPA and RPA, at each bifurcation, the edge with the smallest angle to the previous edge was considered to belong to the LPA/RPA respectively. All other edges were defined as side branches.

For each edge, the length, the area- and perimeter-derived (i.e., hydraulic diameter) and minimal and maximal diameters of the respective vessel segment were obtained. For the MPA and internal edges, the diameters were obtained exactly at the midpoint of each edge. For side branches, the diameters were obtained closer to the outlet nodes. From the minimal and maximal diameters, the mean diameters and ellipticity were calculated. The measurements were accumulated to calculate the overall length and length-weighted diameters of the MPA, LPA and RPA, respectively. Edges with a length below 10 mm were disregarded on the length-weighted diameter calculation, as side branches will likely distort the diameter measurements. The curvature index was calculated from the distance of start- and end-node, divided by the overall length of the considered segment. Lastly, the bifurcation angle between LPA and RPA was determined, by calculating the angle between the vectors connecting the endpoint of the MPA to the endpoint of the first edges of LPA and RPA, respectively, with an overall length of at least 10 mm (see *Figure 6*).

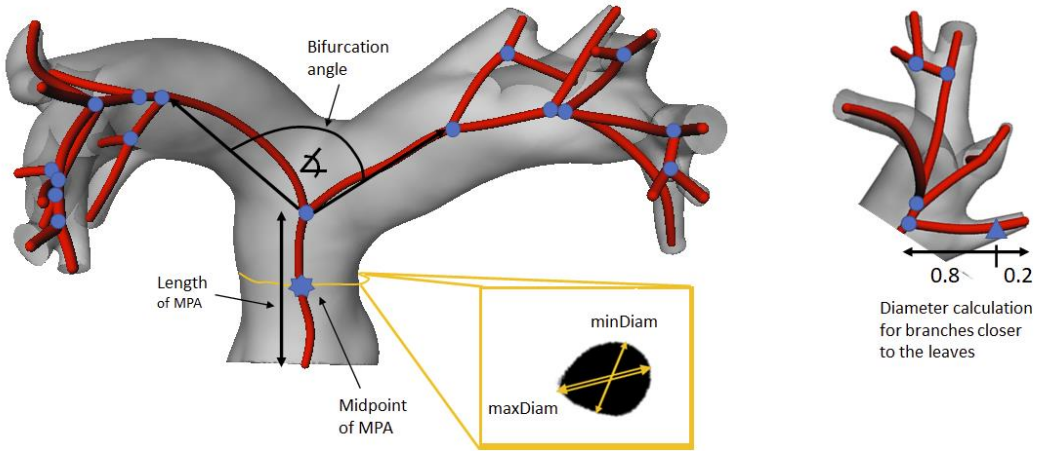

*Figure 6: Measurements from centreline-based analysis: the centreline (red) is subdivided into several edges, connected by nodes (blue), which mark a bifurcation. Diameters for each edge are obtained at the midpoint (blue star) between start and end node of an edge or at start node + 0.8 * (end node - start node) for branches (blue triangle). The bifurcation angle between LPA and RPA is the angle between the vectors connecting the endpoint of the MPA to the endpoint of the first edge of LPA and RPA, respectively.*

Segmentation of the AV using parametric heart model

The segmentation procedure is performed automatically with using a parametric model described earlier[7,8]. However, during the final step, manual correction of the AV leaflets affecting the AV area during fully open state is necessary as the parametric model assumes a symmetric configuration of all three leaflets, which is seldom found in patients with severe aortic stenosis. To assess intra- and inter-operator variability, reconstruction of the AV geometries was repeated by the main operator 6 months after the initial reconstruction. In addition, reconstruction was performed by another user for analysis of inter-operator variability. Based on these segmentations, the AV area was then calculated and compared against each other. *Figure 7* shows the two independent reconstructions of one case exemplarily.

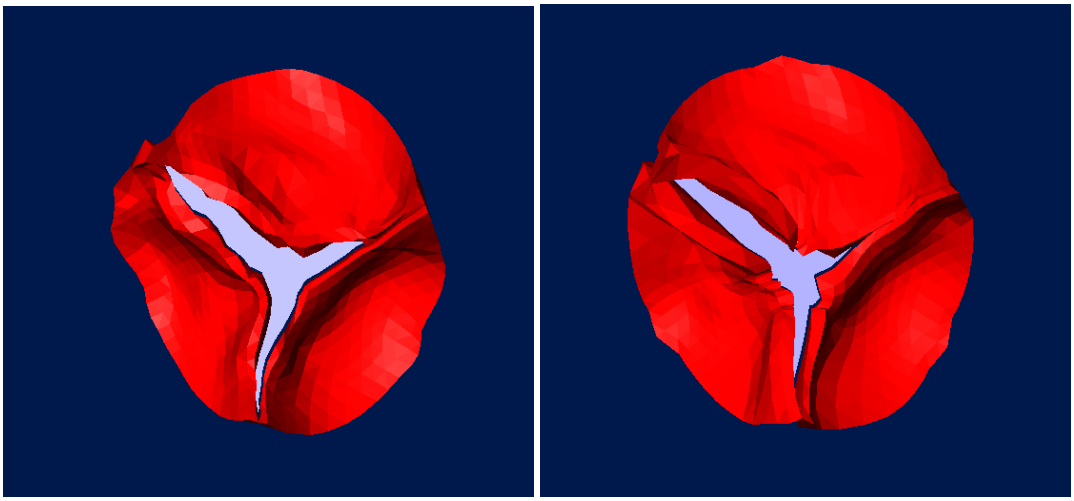

Figure 7: Example of the differences in AV anatomy of one TAVI patient resulting from independent reconstructions by two different operators. The AV area of both operators was 0.58 cm² and 0.42 cm², respectively.

For both analyses, *intraclass correlation coefficients* (ICCs) were calculated according to the convention by McGraw and Wong [ICC (1)[9]]. Only the operator bias on AV area was investigated, as the volume flow rate quantification was based upon the fully automatic segmentation of the LV.

[7] Weese J, Lungu A, Peters J, Weber FM, Waechter-Stehle I, Hose DR. CFD and Bernoulli-based pressure drop estimates: a comparison using patient anatomies from heart and aortic valve segmentation of CT images. Med Phys. (2017) 44:2281–92. doi: 10.1002/mp.12203

[8] Franke B, Weese J, Waechter-Stehle I, Bruning J, Kuehne T, Goubergrits L. Towards improving the accuracy of aortic transvalvular pressure gradients: rethinking Bernoulli. Med Biol Eng Comput. (2020) 58:1667–
79. doi: 10.1007/s11517-020-02186-w

[9] McGraw KO,Wong SP. Forming inferences about some intraclass correlation coefficients. Psychol Methods. (1996) 1:30–46. doi: 10.1037/1082-989X.1.1.30

Quantification of AV calcification

Usually, the AV calcification score is acquired based on CT acquisitions without contrast agent by using a threshold of HU = 130[10]. However, this approach does not allow to measure uncertainty of the calcification measurements. Furthermore, in clinical routine image data with contrast agents as used for TAVI treatment planning is also commonly used for assessment of calcifications, requiring more flexibility in the choice of the HU threshold. Here, currently no agreement for an appropriate HU threshold[11] exists. Since for TAVI planning also dynamic CT acquisition with more than 5 phases per heart cycle are available, this data was used for the uncertainty measurements in calcification measurement. Due to the high contrast of the blood pool, a HU threshold of 800 was chosen for the measurement of the calcification volume. *Figure 8* visualises the process of the calcification volume measurement, which is done in a region of interest covering the AV leaflets and the AV annulus.

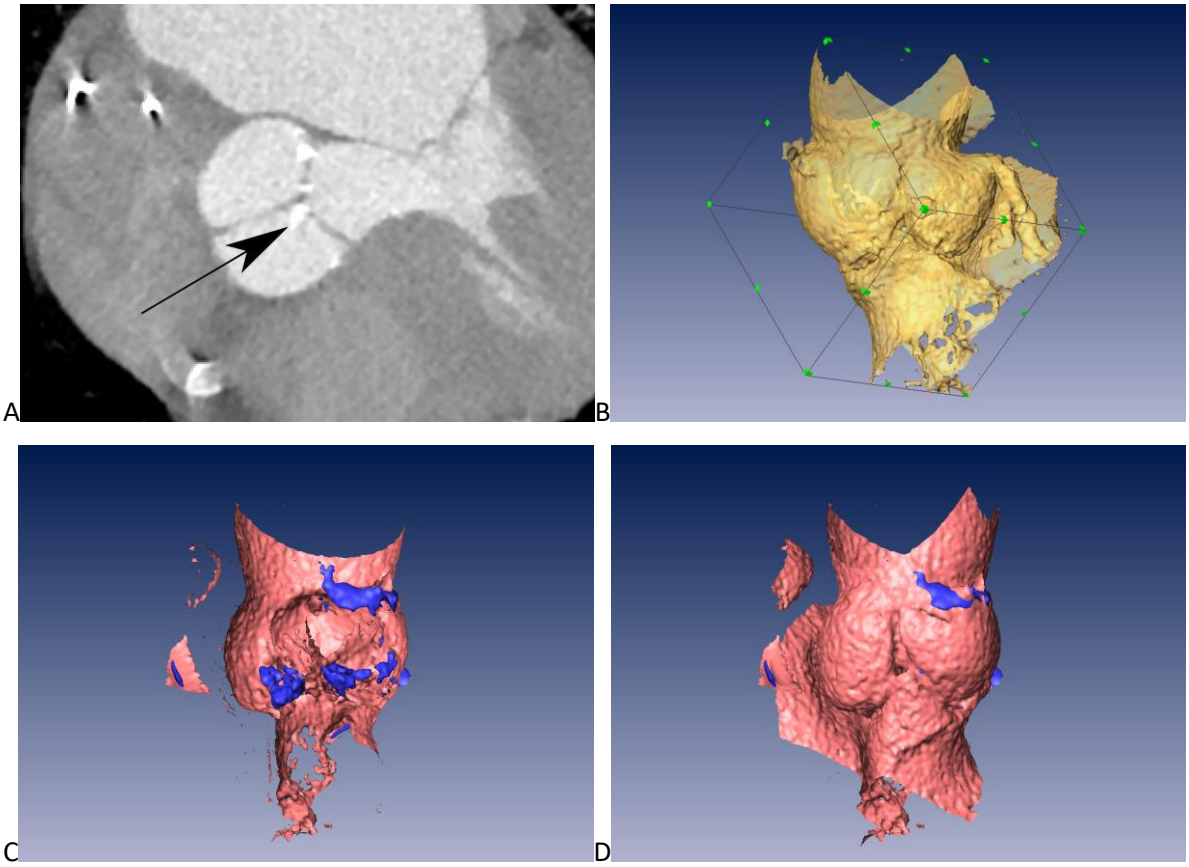

Figure 7: Assessment of AV calcification: (A) - CT image depicting the AV and a black arrow highlighting calcifications with high Hounsfield unit values. (B) - visualisation of the AV as an isosurface with a constant HU of 400 and black wireframe defining the ROI used for the calcification volume measurement. (C) and (D) - frontal and back surfaces of the AV (red) as well as calcifications (blue).

[10] Pawade T, Sheth T, Guzzetti E, Dweck MR, Clavel MA. Why and How to Measure Aortic Valve Calcification in Patients With Aortic Stenosis. JACC Cardiovasc Imaging. 2019 Sep;12(9):1835-1848. doi: 10.1016/j.jcmg.2019.01.045.

Extraction of hemodynamic blood flow information

To simulate blood flow in, for example, patient-specific PA, information about the patient-specific volume flow waveform at the MPA might be required, depending on the question of interest. This information is usually acquired during MRI measurements. Here, data was acquired using a 1.5 T clinical MR system (Achieva; Philips Healthcare, Best, Netherlands) with a five-element cardiac phased-array coil. All flow measurements were performed with automatic correction of concomitant phase errors. 4D MRI was acquired with a field of view of 185 mm x 240 mm x 80 mm, a matrix size of 100 x 128, an acquired voxel size of 2.5 mm x 2.6 mm x 2.5 mm, reconstructed voxel size of 1.9 mm x 1.9 mm x 2.5 mm, repetition time of 3.2 ms, echo time of 1.9 ms, retrospective cardiac gating, flip angle of 5°, number of signal averages of 1 and a velocity encoding of 150 cm/s. The temporal resolution was 25 timesteps. 4D data was analysed using the GTflow (version 3.2.16, Gyrotools, Zurich, Switzerland) as shown in *Figure 9*.

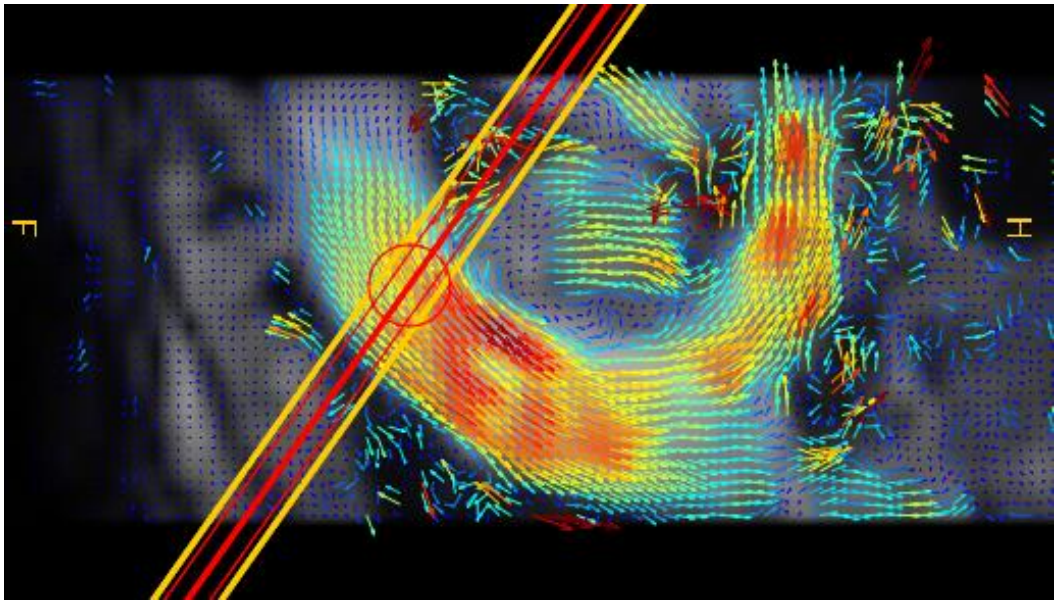

Figure 8: Exemplary 4D velocity encoded MRI velocity vector field in the PA with a measurement plane perpendicular to MPA.

Catheter-based pressure measurements

To simulate the paravalvular leakage after TAVI implantation information about pressures in the LV and aorta are necessary. The paravalvular leakage is moderated by the paravalvular orifices as well as the pressure gradient oriented from aorta to left ventricle during diastole. This data was acquired during TAVI procedure by catheter-based pressure measurements. These measurements are associated with heart-to-heart beat uncertainty. Catheterization is performed according to the Heart Team decision under local (remifentanil) or general anaesthesia (propofol and remifentanil). Blood pressure waveforms (see *Figure 10*) are measured in the ascending aorta as well as in the LV using a 6-F pigtail catheter (Cordis, Dublin, Ireland). Measurements in the ascending aorta are always performed before measurements in the left ventricle. For each measurement, 5 consecutive cardiac cycles or more, if possible, were acquired in order to assess pressure uncertainty. The peak systolic pressure in the left ventricle and the ascending aorta are calculated as the average of all peak values. Peak systolic values at each heart cycle are identified automatically by using MATLAB. Beside measurement of pressure values, for the modelling of paravalvular leakage, information on the duration of the diastolic and/or systolic period is important. These measurements are also based on pressure curves. Please note that the uncertainty in the pressure measurement procedure cannot be assessed via this approach, as due to the retrospective nature of the data only the already filtered and printed pressure waveforms were available.

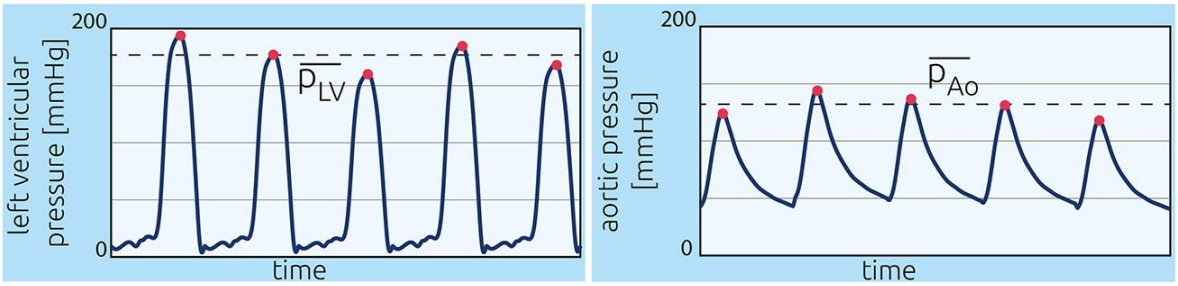

Figure 9: Exemplary catheter-measured pressure curves in the left ventricle (left) and the ascending aorta (right). Red dots mark peak systolic values.

Uncertainty quantification of segmentations

Uncertainty quantification of manually segmented PA surfaces

In *Table 3* results of the surface distances for all 10 investigated cases are summarised, along with the size of each bounding box representing the reconstructed domain, as well as the size of the ROI used for the analysis. On average, 73% ± 8% of the reconstructed domains were considered for the surface distance analysis. While this sounds like a relevant difference, slight changes in the length of branching vessels can result in relevant differences in the bounding box. Also, the region of interest included the entire valid implantation zone in all 10 cases. The averaged surface distance for all cases was 0.39 mm ± 0.22 mm, which is below the average voxel size of 0.596 mm in our data. This means that the uncertainty due to manual segmentation is lower to acquisition accuracy (spatial resolution of the voxel field). The mean Hausdorff distance was 3.7 mm ± 1.06 mm. Large differences were only found for the branching vessels, but not for the main vessels (MPA, LPA, RPA). Finally, regression analysis indicated no significant correlation between averaged surface and Hausdorff distances.

Case	BB (mm x mm x mm)	ROI (mm x mm x mm), (BB/ROI, %)	Surface distance (mm)	HD (mm)
1	126x114x75	104x114x65 (71%)	0.10 ± 0.20	2.97
2	123x125x75	105x110x75 (75%)	0.70 ± 0.33	3.41
3	113x88x54	113x88x47 (87%)	0.17 ± 0.19	2.49
4	163x131x80	125x131x80 (77%)	0.26 ± 0.23	2.70
5	131x97x57	107x88x57 (74%)	0.45 ± 0.44	5.45
6	123x96x64	94x86x64 (68%)	0.25 ± 0.24	4.42
7	130x129x65	107x124x65 (79%)	0.76 ± 0.27	2.49
8	129x105x71	113x90x71 (75%)	0.44 ± 0.43	4.88
9	168x93x100	142x78x90 (64%)	0.29 ± 0.35	3.92
10	143x108x88	110x108x66 (58%)	0.50 ± 0.51	4.51

Table 3: Analysis of the surface distances between manual PA reconstructions of 10 human cases by 2 independent operators in a limited region of interest which represents only the most relevant anatomical region including main, left, and right PA but not all branching vessels.

Uncertainty quantification of geometric parameters: manual PA reconstruction

For all investigated geometric parameters we found no significant differences between both operators (paired t-Student test, $p >> 0.05$), whereas linear regression analysis found significant correlations (all $p < 0.001$) between geometric parameters calculated from surface reconstruction based on the manual reconstructions of both independent operators. *Figure 11* exemplary shows scatter plots for four geometric parameters at different PA vessels (RPA-LPA bifurcation angle, length of the MPA segment, diameter of the LPA segment and the curvature index of the RPA).

To quantify uncertainties, we calculated differences between parameters based on segmentations of two different operators and calculated the *relative uncertainty* (RU) in percentage in two ways:

1. RU_1: relationship of the standard deviation of all 10 differences between calculated values of a geometric parameter divided by the mean parameter value calculated from all 20 values of the same parameter (10 patients, 2 operators) in percentage;
2. RU_2: relationship of the mean absolute differences between calculated values of one geometric parameter divided by the mean parameter value calculated from all 20 values of the same geometric parameter (10 values, 2 operators) in percentage.

Both RU, calculated for four geometric parameters, are shown in *Figure 11* and are summarised in *Table 4*. Finally, we demonstrated that no significant linear regression correlation between surface or Hausdorff distances and differences in calculated geometric parameters occurred due to the different

manual segmentations. The highest relative uncertainty of approximately 10% was found for the diameter (LPA diameter) and corresponds approximately to the three averaged voxel sizes of 0.595 mm, which is still relatively small given the large average value of that parameter.

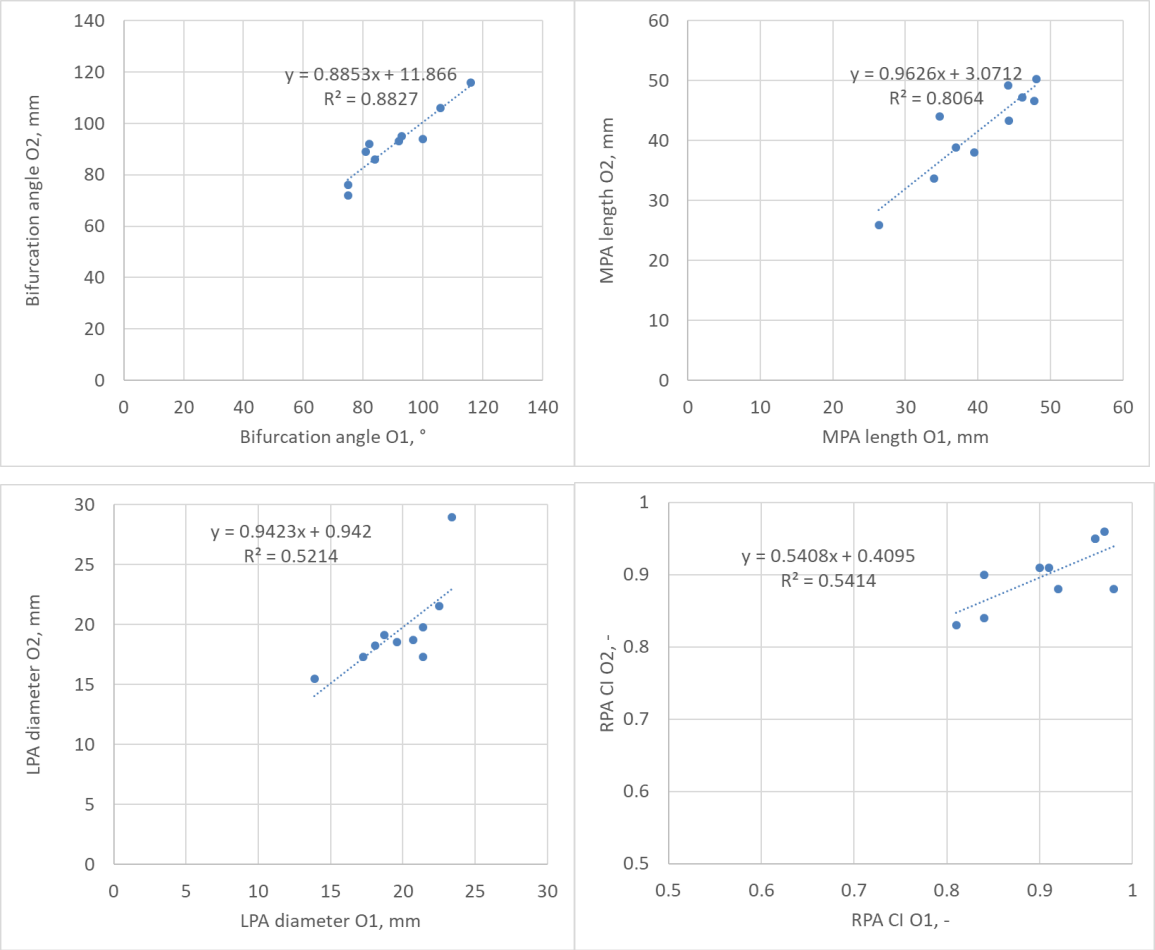

Figure 10: Scatter plots and linear regression analysis for four exemplary geometric parameters describing the PA anatomy. Operator 1 - O1. Operator 2 - O2. Curvature index - CI.

Uncertainty	MPA L	α	LPA D	RPA CI
RU_1	8.2%	5.1%	13.0%	4.6%
RU_2	5.8%	3.6%	9.0%	2.9%
Mean parameter value	40.95 mm	91°	19.59 mm	0.905

Table 4: Relative uncertainties due to manual segmentations performed by two operators of the four exemplary geometric parameters: MPA length (L), bifurcation angle (α) between left and right PA, LPA diameter (D), and RPA curvature index (CI).

Uncertainty quantification of PA surfaces: manual vs. automatic reconstruction

In *Table 5* results of the surface distances for 10 investigated PA cases are summarised in an identical manner as in the previous section. However, here, the surfaces between the first operator's manual reconstruction and the automated reconstructions are compared. On average, 74.5% ± 11.8% of the reconstructed domain were considered for the surface distance analysis. The averaged surface distance for all cases was 0.73 mm ± 0.23 mm, which is slightly larger than the average voxel size of 0.596 mm- This means that the uncertainty due to type of segmentation (manual or automatic) is similar to the acquisition accuracy (spatial resolution). The mean Hausdorff distance was 4.7mm ± 0.88mm.

Case	BB (mm x mm x mm)	ROI (mm x mm x mm), (BB/ROI, %)	Surface distance (mm)	HD (mm)
1	126x114x75	95x114x68 (68%)	0.45 ± 0.41	3.91
2	123x125x75	123x125x63 (84%)	0.32 ± 0.36	4.42
3	113x88x54	104x88x54 (92%)	0.82 ± 0.42	3.58
4	160x131x80	136x77x80 (50%)	0.55 ± 0.53	5.91
5	131x97x57	92x97x57 (70%)	0.75 ± 0.57	4.24
6	123x96x64	108x96x64 (88%)	0.73 ± 0.55	4.31
7	130x129x65	115x106x65 (73%)	0.92 ± 0.57	4.06
8	129x105x71	96x105x71 (74%)	0.84 ± 0.64	4.95
9	168x93x100	150x77x100 (74%)	0.98 ± 0.78	5.72
10	143x108x88	143x78x88 (72%)	0.98 ± 0.88	5.98

Table 5: Analysis of the surface distances between manual and automatic PA reconstructions of all 10 human cases in a limited region of interest which represents only the most relevant anatomical region including main, left, and right PA but not all branching vessels.

Uncertainty quantification of PA geometric parameters: manual vs. U-net segmentations

Similar to the analysis of differences between manual surface reconstruction performed by two operators, geometric parameters based on the manual reconstruction performed by Operator 1 and the automatic reconstruction (see *Table 6*) were compared. The uncertainty of geometric parameters between manual and automatic reconstruction was higher for vessel lengths, diameters, ellipticity, and curvature index compared to the uncertainty due to manual segmentations by two operators. This is due to the data used to train the neural network, which included the entire PA tree up to the 7th - 9th bifurcation generation. In contrast, the manual segmentations were done only until the 3rd or partially 4th generation. Respectively this results in different lengths for PA segments, a difference which propagates further into the definition of the mean diameter and curvature index.

Uncertainty	LPA L	α	LPA D	RPA CI
RU_1	25.5%	3.4%	15.3%	8.8%
RU_2	18.7%	2.9%	11.2%	8.0%
Mean parameter value	98.60mm	91°	19.62mm	0.888

Table 6: Relative uncertainties due to manual reconstruction performed by Operator 1 and automatic reconstructions, calculated for four exemplary geometric parameters: main PA (MPA) length (L), bifurcation angle (α) between left and right PA (RPA), LPA diameter (D), and RPA curvature index (CI).

Uncertainty quantification of the AV area

Intraclass correlation coefficients calculated for the intra- and interobserver analyses were 0.99 and 0.88, indicating an excellent intraobserver reliability and a good agreement between different observers. The relative uncertainty of the intraobserver bias defined as standard deviation of the differences between AV areas based on two reconstructions performed by the same with a time delay of 6 months was 7.42% and thus lower than the interobserver-based relative uncertainty of 12.76%.

Uncertainty quantification of the AV calcification volume

Table 7 summarises the calcification volumes averaged for each patient over all acquired heart phases as well as the resulting relative uncertainty. It seems that with increasing calcification volume the relative uncertainty decreases, while the absolute uncertainty (i.e., the standard deviation) remains stable. Note that the calcification volume was defined as volume of voxels with HU above 800.

TAVI case	N of CT phases	Calcification volume (mean±s.d.), (mm)	RU (%)
1	11	11514 ± 888	7.7
2	11	51543 ±517	1.0
3	10	3672 ± 693	18.9

Table 7: Results of the calcification volume quantification and resulting RU exemplary for 3 TAVI patients.

Uncertainty quantification of PA flow rates

In order to quantify uncertainty of the flow rate measurements by 4D flow MRI, the flow rate was measured at 10 different planes along the centreline of the MPA as visualised in *Figure 12*. The measurements were performed in three different subjects. *Table 8* summarises, for each subject, the cycle-averaged flow rate, the averaged peak-systolic flow rates, as well as the relative uncertainty for both hemodynamic parameters defined as the ratio of the standard deviation of all ten measurements and the mean of all 10 measurements.

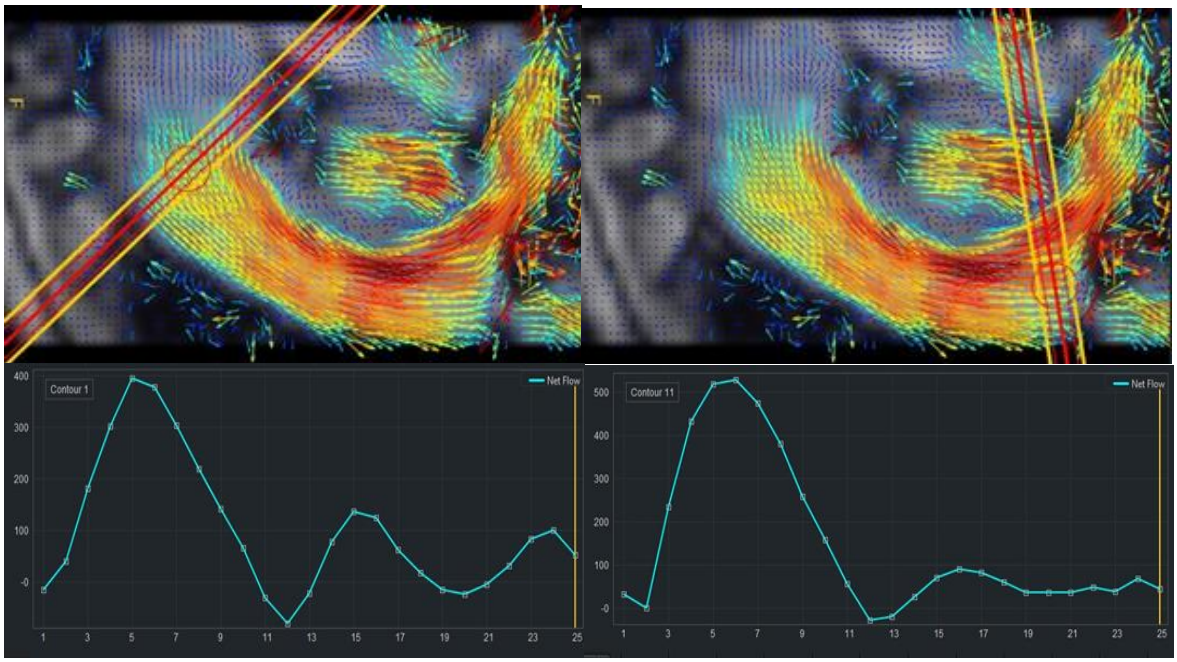

Figure 11: Left: the first plane for flow rate measurement in the MPA together with the measured flow rate curve. Right: The last plane for the MPA flow rate measurements with the respective curve.

Case	mean Q with s.d. (ml/s)	peak-systole Q with s.d. (ml/s)	$RU_{mean\text{-}Q}$ (%)	$RU_{peak\text{-}systole\text{-}Q}$ (%)
1	127 ± 6.0	459 ± 28.1	4.8%	10.8%
2	100 ± 8.4	309 ± 62.4	8.4%	20.2%
3	130 ± 15.2	503 ± 49.2	11.7%	9.8%

Table 8: Exemplary PA flow rates measured for three subjects. Mean and peak-systolic flow rates averaged over measurements in 10 different planes along the MPA, as well as the relative uncertainties calculated for both parameters.

Uncertainty analysis of catheter-measured pressure curves

The average and standard deviation of the peak systolic, static pressure measured in the LV and the ascending aorta of TAVI patients investigated in SIMCor was 162.7 ± 32.4 and 113.1 ± 25.0 mmHg. For 5 randomly selected TAVI cases, the peak systolic LV pressures as well as systolic phase period and relative uncertainty of these 2 parameters are summarised in *Table 9*.

TAVI case	Peak systole P (mmHg)	RU_P	Systolic time T (s)	RU_T
1	157 ± 1.6	1.0%	0.48 ± 0.010	2.10%
2	159 ± 4.0	2.5%	0.71 ± 0.01	2.14%
3	134 ± 3.0	2.3%	0.59 ± 0.011	1.93%
4	127 ± 1.5	1.2%	0.45 ± 0.016	3.68%
5	147 ± 1.2	0.8%	0.51 ± 0.006	1.3%
Mean	**144.8**	**1.56%**	**0.548**	**2.23%**

Table 9: Peak systolic pressures and systolic times averaged over catheter-based pressure measurements of five consecutive heart cycles in 5 TAVI patients with resulting RU for pressure and time.

Conclusions

The overall uncertainty introduced due to image processing methods is relatively low. The inter- and intra-operator reliability for the manual reconstruction of the aortic or PA geometries was excellent and observed differences were below or equal to the image data resolution. Measurement of functional parameters was also found to be robust with respect to the uncertainties to be expected in clinical real-world data. Nonetheless, the propagation of these uncertainties throughout the modelling pipelines for device implantation and device effect simulation is a necessary validation step and will be investigated in subsequent analyses.

Appendix

List of tools used for uncertainty quantification

N	Tools	Aim
1	ZIBAmira (v. 2015.28, Zuse Institute Berlin, Germany)	Manual or semi-automatic segmentation, medical image data visualisation
2	MeVisLab software (MeVis Medical Solutions AG, Germany)	Automatic centerline-based analysis of geometric parameters.
3	IBM SPSS Statistics 28 software (IBM Company, USA)	Statistical analysis of all data.
4	GT Flow program (version 3.2.16, Gyrotools,Zurich, Switzerland)	Analysis of MRI measured velocity vector fields.
5	MATLAB and Statistics Toolbox Release 2012b (The MathWorks, Inc., Natick, Massachusetts, United States)	Analysis of pressure curves

Table 10: List of used tools.

List of parameters used for uncertainty quantification

N	Use case	Parameter type	Parameter
1	TAVI	Geometric	AV area, cm^2
2	TAVI	Geometric	Volume of calcifications, mm^3
3	TAVI	Hemodynamic	LV pressure, mmHg
4	TAVI	Hemodynamic	Systolic time, s
5	PAPS	Geometric	Mean surface and Hausdoff distances, mm
6	PAPS	Geometric	MPA/LPA/RPA lengths, mm
7	PAPS	Geometric	MPA/LPA/RPA diameters, mm
8	PAPS	Geometric	Ellipticity/Curvature indexes, -
9	PAPS	Geometric	LPA-RPA bifurcation angle, °
10	PAPS	Hemodynamic	PA peak systolic flow rate, ml/s
11	PAPS	Hemodynamic	PA mean flow rate, ml/s

Table 11: List of investigated parameters.